Ducea, M.N., et al., 2022, Diapirism of carbonate platforms subducted into the upper mantle: Geology, v. 50, https://doi.org/10.1130/G50000.1

Diapirism of carbonate platforms subducted into the upper mantle

Ducea et al., Supplementary Material

METHODS

Numerical Models

The SOPALE numerical code is used to model the coupled thermal-mechanical evolution of the lithosphere-upper mantle system. This code uses arbitrary Lagrangian-Eulerian finite element methods to solve the equations of conservation of mass, momentum and energy, assuming plane strain and incompressible materials (Fullsack, 1995). The two-dimensional model domain is 2000 km wide and 600 km deep. The Eulerian finite element mesh has element widths of 10 km everywhere and element heights of 1 km in the upper 100 km, 2 km between 100 and 150 km depth, and 18 km below. Resolution tests show that this distribution of elements accurately captures the dynamics in the area of interest (mantle wedge corner), while allowing the models to run in a reasonable length of time within the memory constraints of the computer system.

The initial model geometry shown in Figure S1. The models consist of an oceanic plate between two continental plates. The oceanic plate includes a 1 km thick layer of carbonate, 7 km oceanic crust, and 64 km mantle lithosphere. The total oceanic plate thickness is 72 km, corresponding to a ~30 Ma oceanic plate, as inferred for Tethyan subduction based on the Mesozoic geology of the Carpathians or Alps. The interiors of both continental plates have a 24 km upper crust and 12 km lower crust. The continent on the left has a total thickness of 200 km and is separated from the oceanic plate by a 200 km wide continent margin region where the lithosphere and crustal thicknesses taper to the oceanic values. This plate is carried into the subduction zone during plate convergence and thus is called the lower continental plate. The continental plate on the right forms the upper plate in the model and has an initial total lithosphere thickness of 50 km, consistent with its position above a subducting plate (Currie and Hyndman, 2006). The initial plate boundary between the oceanic and upper continental plates includes weak seed that facilitates the initiation of subduction.

Table S1 gives the thermal and mechanical properties of model materials. All materials have a temperature-dependent density and viscous-plastic rheology, using parameter values

based on earlier studies (e.g., Beaumont et al., 2006; Currie et al., 2007). Thermal conductivity is constant and radioactive heat production is included in only the upper and lower continental crusts. Models include a phase change for the oceanic crust as it enters the eclogite stability field, such that its density increases but no other properties are changed (Currie et al., 2007). Frictional-plastic deformation is modelled using a Drucker-Prager yield criterion that includes strain softening. At stresses below plastic yield, deformation is viscous using rheological parameters from laboratory-derived flow laws. A scaling factor (f) is used to linearly increase/decrease the effective viscosity, to allow for changes in strength owing to minor variations in the composition or hydration state relative to the laboratory materials (e.g. Beaumont et al., 2006). The upper continental crust uses a wet quartzite flow law (Gleason and Tullis, 1995) with f=5. The lower continental crust and oceanic crust use the rheology of dry Maryland diabase (Mackwell et al., 1998) with f= 0.1. All mantle materials use a wet olivine rheology (Karato and Wu, 1993). The sublithospheric mantle has f=1. The mantle lithosphere of the oceanic and lower continental plates has f=10, to approximate relatively dry and strong mantle lithosphere. The mantle lithosphere of the upper continental plate has f=1, assuming that this material is hydrated by the subduction zone. As a result, this material has the same rheology as the sublithospheric mantle. In Figures 1, Figure S2, and Animation 1, the initial continental mantle lithosphere is shaded grey to allow this material to be tracked during model evolution.

The focus of this study is the carbonate layer atop the oceanic plate. The layer is assumed to be predominantly carbonate, mixed with 20% pelagic and terrigenous sediments. The density of this layer is 2700 kg/m^3 at 200°C, making it 100 kg/m^3 less dense than upper continental crust and ~650 kg/m^3 less dense than mantle when materials are at the same temperature. Carbonate is generally believed to be weak, although there is uncertainty in its rheological parameters (Schmid et al., 1980, Heard and Raleigh, 1972). For simplicity, the models use the rheological parameters of wet quartzite (Gleason and Tullis, 1995) for the carbonate layer, with a scaling factor of f=0.1, such that the effective viscosity of carbonate is a factor of 10 less than that of quartzite.

Models are initiated by first determining the initial 2D thermal structure, based on the thermal properties and geometry of all materials. A high conductivity (k=128 W m^{-1} K^{-1}) is used in the sublithospheric mantle to ensure that it has an initially adiabatic temperature; after the initial structure is determined, the thermal conductivity is 2.25 W m^{-1} K^{-1} for later calculations. Figure S1 shows the initial geotherms for each plate, where the conductive

geotherms intersect a 1300°C adiabat at the base of the plate. The models then undergo isostatic adjustment and a period of subduction initiation, where 200 km of convergence is applied at the left-hand boundary of the model to create a one-sided subduction zone. The model run starts from this point (time of 0 Myr)

During the model run, the boundary conditions are as follows (Figure S1). The top boundary is stress-free with a temperature of 0°C, and the bottom is a closed, free-slip boundary with a temperature of 1540°C compatible with the adiabatic temperature at 600 km depth. Plate convergence is imposed through applied horizontal velocities on the side lithosphere boundaries. The model has a convergence rate of 2.5 cm/yr, including 1.5 cm/yr of oceanic plate convergence (V_o) and 1 cm/yr of continental plate convergence (V_c). Plate convergence is balanced by a uniform outflow through the sublithospheric mantle side boundaries (V_b ~ 0.31 cm/yr) to ensure mass balance in the model domain. Models are solved in the continental reference frame by adding velocity V_c to all side boundaries. The lithosphere temperatures on the left boundary correspond to a continental geotherm for a 120 km lithosphere thickness (Extended Data Figure 1), and all other side boundaries are insulating (no heat flux).

Reference Model and Additional Models

The reference model uses the parameters in Table S1. The evolution of this model is shown in Figure 1 (main text) and in Animation 1. In Figure S2, the full model domain is shown at three timesteps for this model. The main dynamics occur within the areas shown in Figure 1 and Animation 1. Some minor gravitational instabilities (small-scale convection) occur near continent-ocean transition in the lower plate and near the right-hand model boundary, as shown by the deflections of the 1200°C isotherm. These do not affect the area of interest in the mantle wedge corner. The oceanic plate descends at an angle of 30-40° through the mantle and interacts with the bottom boundary only in the late stages of the model.

Figure S3 shows three additional models that examine variations in key parameters, keeping all other parameters the same as in the reference model (Table S1). Figure 3S-a is a model in which the carbonate layer is both stronger and denser, to test a case where the layer has a greater amount of pelagic and terrigenous sediments. Here, the layer has the rheology of wet quartzite with f=1 and a reference density of 2800 kg/m^3 (i.e., ten times stronger and 100 kg/m^3 denser than the reference model). As in the reference model, the layer is carried into the mantle and buoyantly detaches from the slab. Diapirism initiates ~1 Myr earlier than in the reference model, as the higher viscosity allows for a slightly thicker layer to be transported

atop the slab. However, diapirs are somewhat smaller and less continuous than in the reference model, resulting in a smaller amount of carbonate in the mantle wedge corner.

Figure 3S-b is a model in which the upper plate mantle lithosphere is 10 times stronger than in the reference model, under the assumption that this material is relatively dry. The main effects of the stronger continental mantle lithosphere are: (1) the carbonate diapir is unable to displace this material and accumulates at the base of the continent, rather than at the Moho, and (2) the oceanic crust is forced to fully subduct below the continent. In the reference model, some oceanic crust was emplaced near the upper plate Moho (Figure 1b) before being entrained above the carbonate layer and subsequently mixed in the upwelling diapir (Figure 1c). In contrast, the model with stronger continent mantle lithosphere (Figure 3S-b) has almost no oceanic crust in the carbonate diapir. In addition, there are some continental crust particles in the mantle wedge that appear to be the result of subduction erosion in the early stages of the model.

The effect of a higher convergence rate is shown in Figure 3S-c, where the model panels are shown at the same amounts of convergence as in models with 2.5 cm/yr. This model uses a convergence rate of 4 cm/yr, including 1 cm/yr continental plate motion. Carbonate diapirs readily form in this model, although they are narrower than in the reference model, as the higher convergence rate causes a greater shearing and entrainment (Currie and Beaumont, 2011). In addition, the larger convergence rate creates a stronger mantle wedge corner flow, resulting in circulation of the detached carbonates in the corner and reduced intrusion in to the backarc.

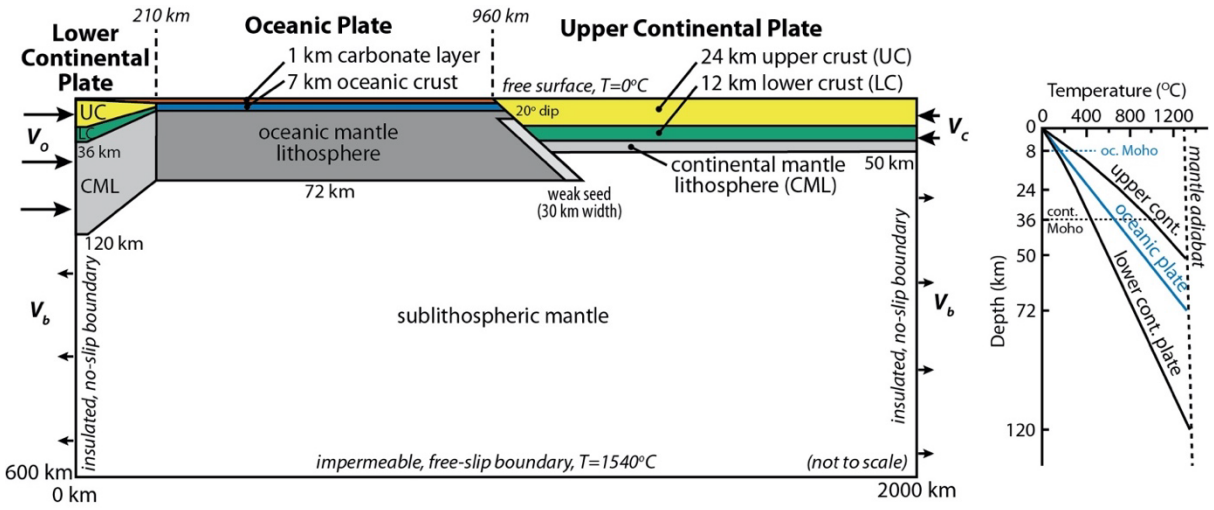

Figure S1. The initial geometry of the numerical models and boundary conditions (left) and initial geotherms applied to the lithosphere of the three regions (right).

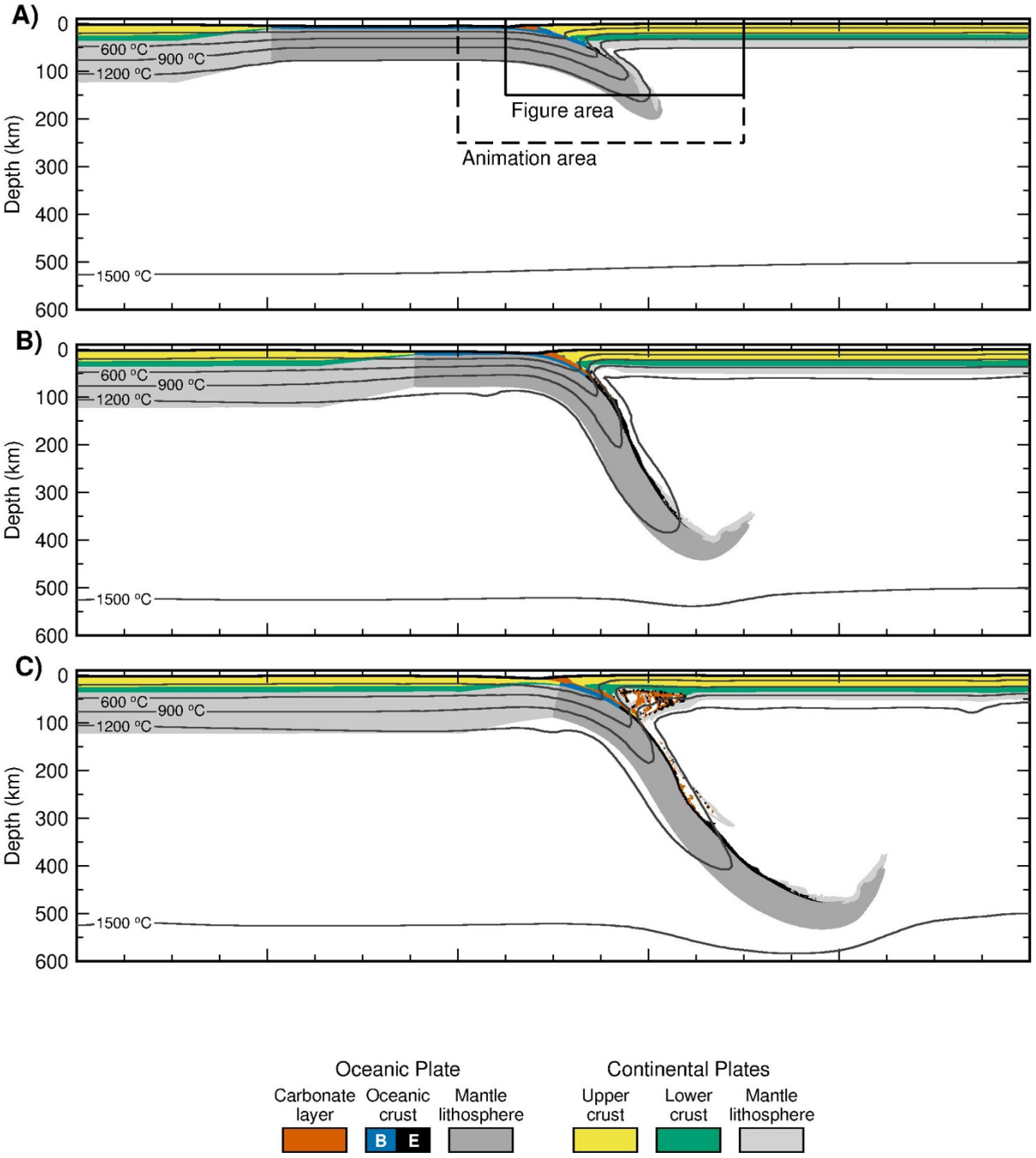

Figure S2. Evolution of the reference model showing the full model domain at model times of a) 0 m.y., b) 12 m.y., and c) 24 m.y. B=basalt; E=eclogite.

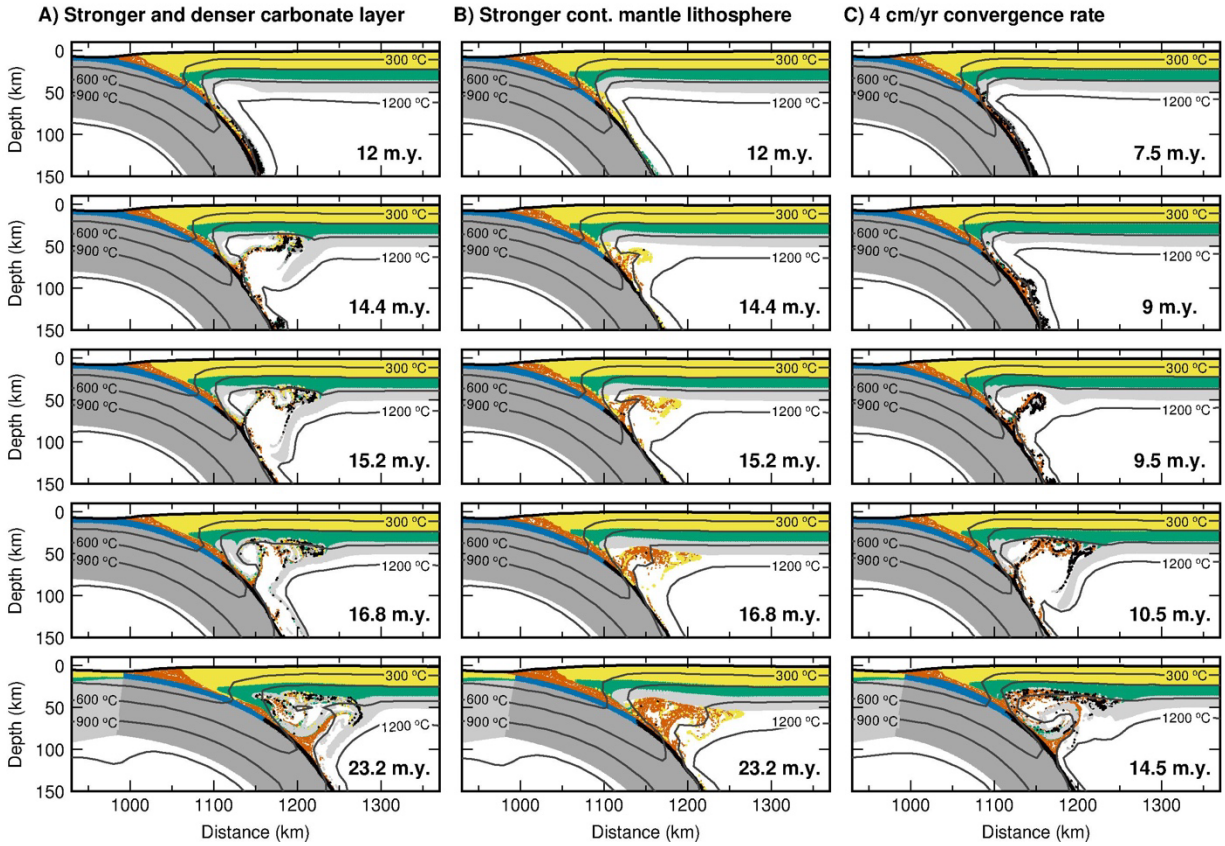

Figure S3. Evolution of additional models that test variations in key parameters: a) a carbonate layer that is 10x stronger and 100 kg/m^3 denser than the reference model, b) an upper plate mantle lithosphere that is 10x stronger than the reference model, and c) a higher convergence rate (4 cm/yr vs. 2.5 cm/yr for the reference model). Note that each row shows the models at the same amount of convergence: 300 km, 360 km, 380 km, 420 km and 580 km (from top to bottom). Material colors follow those used in Figure S2. Cont.=continental

Table S1. Material properties for the reference model.

	Carbonate layer	Oceanic crust	Oceanic mantle lithosphere	Continental upper crust	Continental lower crust	Continental mantle lithosphere	Sublith. mantle
Plastic rheology[a]							
c_0 (MPa)	20	0	0	20	0	0	0
ϕ_{eff}	15º to 2º	15º to 2º	15º to 2º	15º to 2º	15º to 2º	15º to 2º	15º to 2º
Viscous rheology[b]							
f	1	0.1	10	5	0.1	10 (lower), 1 (upper)	1
B* (Pa $s^{1/n}$)	2.92×10^{6}	1.91×10^{5}	1.92×10^{4}	2.92×10^{6}	1.91×10^{5}	1.92×10^{4}	1.92×10^{4}
n	4.0	4.7	3.0	4.0	4.7	3.0	3.0
Q (kJ mol^{-1})	223	485	430	223	485	430	430
V* (cm^3 mol^{-1})	0	0	10	0	0	15	15
Thermal parameters[c]							
k (W m^{-1} K^{-1})	2.25	2.25	2.25	2.25	2.25	2.25	2.25
A (μW m^{-3})	0	0	0	1.0	0.4	0	0
c_p (J kg^{-1} K^{-1})	750	750	1250	750	1250	1250	1250
Density[d]							
ρ_0 (kg m^{-3})	2700	2950	3250	2800	2900	3250	3250
T_0 (ºC)	200	500	1330	200	500	1330	1330
Eclogite ρ_0 (kg m^{-3})	--	3450	--	--	--	--	--
Eclogite T_0 (ºC)	--	500	--	--	--	--	--
α (K^{-1})	3.0×10^{-5}	3.0×10^{-5}	3.0×10^{-5}	3.0×10^{-5}	3.0×10^{-5}	3.0×10^{-5}	3.0×10^{-5}

[a] Frictional-plastic deformation follows a Drucker-Prager yield criterion: $J'_2 = c_0\cos\phi_{eff} + P\sin\phi_{eff}$, where where c_0 is the cohesion, ϕ_{eff} is the effective internal angle of friction, and J'_2 is the square root of the second invariant of the deviatoric stress tensor. Strain softening is included through a linear decrease in ϕ_{eff} over accumulated strain of 0.5 to 1.5.

[b] The effective viscosity (η_{eff}) for viscous deformation is given by: $\eta_{eff} = f(B^*)\left(\dot{I}_2\right)^{(1-n)/n}\exp\left(\frac{E^*+PV^*}{nRT}\right)$, where $\dot{I}_2$ is the square root of the second invariant of the strain rate tensor, P is the total pressure, T is the temperature, f is a scaling factor, n is the stress exponent, E^* is the activation energy, V^* is the activation volume and R is the universal gas constant. B^* is the pre-exponential factor and includes a conversion from the uniaxial laboratory experiments.

[c] Thermal properties are the thermal conductivity (k), radiogenic heat production (A) and specific heat capacity (c_p).

[d] Density varies with temperature: $\rho(T) = \rho_0\left(1 - \alpha(T - T_0)\right)$, where ρ_0 is the reference density at temperature T_0 and α is the volumetric thermal expansion coefficient.

Physical Properties and Melting Calculations

To predict seismic velocities (V_p, V_s) and other physical parameters, we use an updated Excel© macro (Abers and Hacker, 2016) that uses Hacker and Abers (2004) algorithm, over a reasonable range of temperatures (1000-1400ºC) and pressures (10 – 40 kbar). Calculations start with a dry peridotite (Ernst, 1978) and mixed progressively with modal 5, 10, 15 and 20% $CaCO_3$ which results in linear (or planar in P-T-V_p space) arrays of seismic velocities that progressively decreases. Calculated V_p (km/s) anomalies relative to the dry peridotite (Figure S4) show that over the mentioned ranges of temperatures and pressures these mixtures has as much as 3% lower velocities.

Forward modelling of partial melting was carried out using pMELTS engine (Ghiorso et al., 2002). Starting composition consist of dry (Hirose and Kushiro, 1993) and wet (0.5wt% H_2O) peridotite (average natural lherzolite with no carbonate in it), mixed with 2.5% to 15% $CaCO_3$, in increments of 2.5%. Calculations were done within 10 kbar – 30 kbar pressure range and 900ºC – 1300ºC temperature range at NNO oxygen fugacity. Modelling assumed no fractionation of solids, liquids or fluids. Each mixture, dry or wet, was run at constant pressure starting with 1 GPa in steps of 0.5 GPa with 3ºC increments from initial to final temperature. The presence of carbonate in the dry peridotite mix produces a gradual increase in melt fraction up to 12% at 10% carbonate in the mix, especially in the low P – high T region. However, melt fraction does not exceed 4% between 1.5-2.5 GPa. The presence of 0.5% H_2O further increases melt fraction, although not significantly. However, melt production is boosted up in the low P – high T region (e.g. 1 GPa and 1250-1300ºC), to as high as 18% at 10% carbonate in the mix. Melt compositions tend to become highly carbonatic as pressure increases, the presence of water having a tendency of lowering CO_2 concentration in the melt. However at 2.5 GPa, melts are calcio-carbonatites or highly undersaturated feldspathoid bearing leucitite and phonolites.

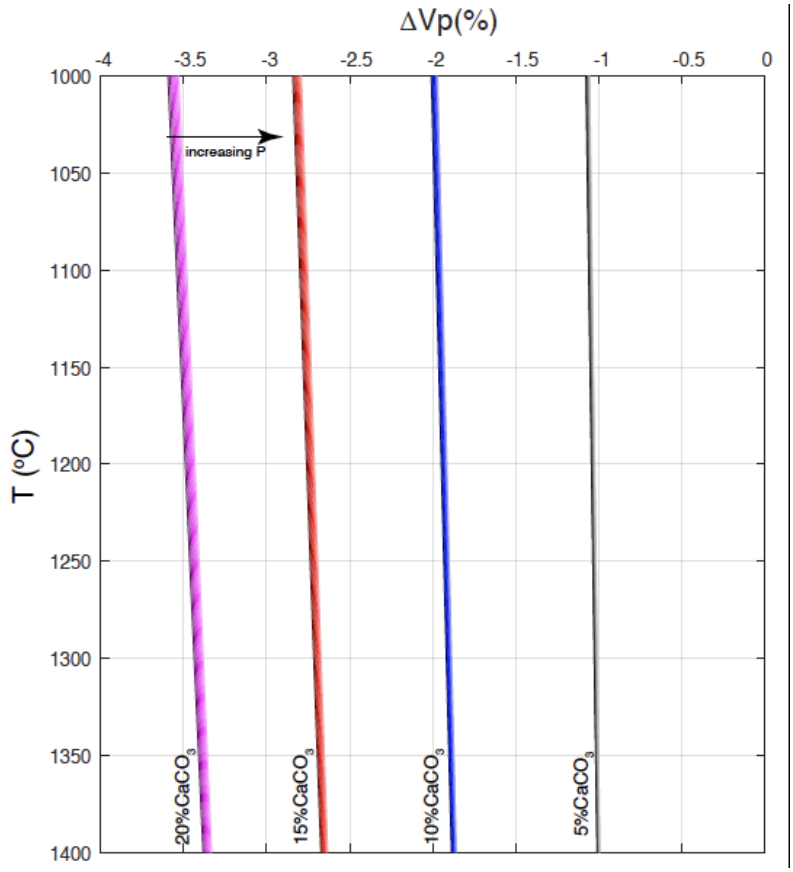

Figure S4. V_p anomalies calculated for a dry peridotite mixed with 5% to 20% $CaCO_3$. Anomalies are calculated as differences of % V_p for a particular composition relative to a carbonate free peridotite and are expressed as negative numbers. Each linear array, corresponding to the specified carbonate proportions in the mix, represents a set of V_p curves for a range of pressures between 10 – 40 kbar (in increments of 5 kbar), increasing in the direction of fading color, marked by the black arrow.

Geologic Constraints from the Tethyan Realm

Mesozoic and Cenozoic carbonate sequences are ubiquitous in the Tethyan realm. The ultimate closure of various oceans and back arc basins of the Neo-Tethys led to the development of the Alpine-Carpathian-Balkan chain, as well as the Appenines and Dinarides in Europe (Schmid et al., 2020). More carbonate sequences (including carbonate platforms) cover much of the undeformed continental margins of Europe (Pall et al., 2018) and are very commonly caught in the fold and thrust belts of the Alpine orogen in Europe (Trumpy, 2001).

The extent, geometry and thickness of these carbonate sequences, both spatially and temporally are difficult to evaluate as their variations in the surfaces of deposition were controlled by the variations of the changing architecture of submarine basins and by the dynamic of the former living systems (as carbonate producing organisms). The living systems

producing carbonate deposits were biologically reactive at the changes of depositional environment (e.g. locally induced palaeoecological changes in a particular depositional setting) and/or to globally physical changes in the Earth's biosphere (Schlager, 1991; Pomar and Kendall, 2008; Van Buchem et al., 2010). Therefore, in order to have a general image on the amounts of carbonates that could be involved in subduction systems, we consider that carbonate sequences reveal specific stratigraphic features. For the estimations of the extent and thickness of these carbonate sequences, the chronological aspects should be considered (Markello et al., 2008; Van Buchem et al., 2010). Gerdes et al. (2010) discussed the influence of basin architecture and eustacy in the evolution of Tethyan Mesozoic and Cenozoic carbonate sequences, concluding that the volume of available accommodation space and the formation of large carbonate sequences increase during specific time-intervals of the Triassic and Jurassic and reached a maximum during the Late Cretaceous and later these have been progressively reduced during the Cenozoic. Within these large carbonate sequences involved in the subduction systems, the carbonate platforms particularly contributed with significant amounts of pure carbonates in these systems. We are using here the term "carbonate platforms" for shallow-water carbonate sequences including ramps and rimmed shelves developed along continental margins (Kiessling et al., 2010). Most of the carbonate platforms were deposited over millions to tens of millions of years and were affected by gaps in sedimentation and drowning episodes.

Pall et al. (2018) produced an estimation of the lengths of the subduction zones intersected by carbonate platforms at different time intervals during the Phanerozoic, based on plate paleogeographic reconstructions and presumed distribution of carbonate platforms. They showed that during the last 250 Ma until the present, 70% of total global subduction zone lengths were intersected by ancient carbonate platforms. While the full extent of these carbonate platforms that were likely similar in size and thickness with the Great Australian barrier reef (up to over 400 km wide and over 2000 km long) or with the Bahama Carbonate Platform (up to 700 km north-south and 300 km east-west) is impossible to reconstruct for the Mesozoic and Cenozoic in the European realm, it is clear from geologic observations alone that much of these structures did intersect various trenches of the Alpine Tethys, Neo-Tethys and the modern Mediterranean, etc (Schmid et al., 2020). Much of these have gone missing as they were subducted with their thinned continental or narrow oceanic plates and the fate of these materials is unknown.

Bosscher and Schlager (1993) published an overview concerning the accumulation rates of the most extensive carbonate platforms in the Phanerozoic. The authors compiled numerous data from published literature and listed the thickness of carbonate platforms considering only pure shallow water carbonates bodies (excluding deeper water carbonates and/or significant intercalations of siliciclastic sediments). Thus, the stratigraphic thickness of carbonate platforms was highly variable, between 1.3 - 2 km in Triassic (e.g. in the Alps, Austria, Italy), 0.6 - 2 km in Jurassic (e.g. Argentina, Italy, Slovenia, Caucasus), 0.3 - 4 km in Cretaceous (e.g. in Italy, Spain, France, Iraq, Mexico), 0.2 - 4 km in Cenozoic (e.g. in Italy, Lebanon, French Polynesia, Brazil). Moreover, during the Middle and Late Jurassic to Cretaceous, several km-thick sequences of almost pure shallow-water carbonates were deposited on the Adriatic Carbonate Platform (Juračić et al., 2004). The Panormide Carbonate Platform in western Sicily consists of Upper Triassic to Upper Eocene mostly shallow-water carbonate succession, 1-1.2 km thick (Basilone, 2009). The average thickness of the preserved Upper Jurassic-Lower Cretaceous Getic Carbonate Platform is around 1-1.5 km in the Carpathians (Patrulius, 1976). However, globally carbonate platforms can range in preserved thickness from just a few tens of meters to over 8 km in some Paleozoic platforms from Kazakstan (Pall et al., 2018). The Bahama Carbonate Platforms consists of almost 5 km of shallow-water carbonates (limestone and dolomite with thin evaporates intercalations) since Jurassic to Pleistocene (Tucker and Wright, 1990). Large recent reefs carbonates of the Indian Ocean and western Pacific (Lapointe, 2001) also average about 1 km in thickness.

Most basins of the Neo-Tethys were narrow basins only several (300-600 km) hundred kilometers wide (Roban et al., 2020) and they closed via subduction and collision in relatively short bursts (~ 10 - 20 Myr on average), commonly with limited or in some cases, no magmatism. We conclude that a good average carbonate platform thickness is 1 km.

REFERENCES CITED

Abers, G. A., and Hacker, B. R., 2016, A MATLAB toolbox and Excel workbook for calculating the densities, seismic wave speeds, and major element composition of minerals and rocks at pressure and temperature: Geochemistry, Geophysics, Geosystems, v. 17, no. 2, p. 616-624, doi 10.1002/2015gc006171.

Basilone, L., 2009, Sequence stratigraphy of a Mesozoic carbonate platform-to-basin system in western Sicily: Central European Journal of Geosciences, v. 1, no. 3, p. 251-273, doi: 10.2478/v10085-009-0021-8.

Beaumont, C., Nguyen, M. H., Jamieson, R. A., and Ellis, S., 2006, Crustal flow modes in large hot orogens, *in* Law, R. D., Searle, M. P., and Godin, L., eds., Channel Flow, Ductile Extrusion and Exhumation in Continental Collision Zones Volume Special Publications 268, Geological Society, London, p. 91-145, doi: 10.1144/gsl.Sp.2006.268.01.05.

Bosscher, H., and Schlager, W., 1993, Accumulation Rates of Carbonate Platforms: The Journal of Geology, v. 101, no. 3, p. 345-355, doi: 10.1086/648228.

Currie, C. A., and Beaumont, C., 2011, Are diamond-bearing Cretaceous kimberlites related to low-angle subduction beneath western North America?: Earth and Planetary Science Letters, v. 303, no. 1, p. 59-70, doi: 10.1016/j.epsl.2010.12.036.

Currie, C. A., and Hyndman, R. D., 2006, The thermal structure of subduction zone back arcs: Journal of Geophysical Research: Solid Earth, v. 111, no. B8, doi: 10.1029/2005JB004024.

Currie, C. A., Beaumont, C., and Huismans, R. S., 2007, The fate of subducted sediments: A case for backarc intrusion and underplating: Geology, v. 35, no. 12, p. 1111-1114, doi: 10.1130/G24098A.1.

Ernst, W. G., 1978, Petrochemical Study of Lherzolitic Rocks from the Western Alps*: Journal of Petrology, v. 19, no. 3, p. 341-392, doi: 10.1093/petrology/19.3.341.

Fullsack, P., 1995, An arbitrary Lagrangian-Eulerian formulation for creeping flows and its application in tectonic models: Geophysical Journal International, v. 120, no. 1, p. 1-23, doi: 10.1111/j.1365-246X.1995.tb05908.x.

Gerdes, K. D., Winefield, P., Simmons, M. D., and Van Oosterhout, C., 2010, The influence of basin architecture and eustacy on the evolution of Tethyan Mesozoic and Cenozoic carbonate sequences: Geological Society, London, Special Publications, v. 329, no. 1, p. 9-41, doi 10.1144/sp329.2.

Ghiorso, M. S., Hirschmann, M. M., Reiners, P. W., and Kress, V. C., 2002, The pMELTS: A revision of MELTS for improved calculation of phase relations and major element partitioning related to partial melting of the mantle to 3 GPa: Geochemistry, Geophysics, Geosystems, v. 3, no. 5, p. 1-35doi: 10.1029/2001gc000217.

Gleason, G. C., and Tullis, J., 1995, A flow law for dislocation creep of quartz aggregates determined with the molten salt cell: Tectonophysics, v. 247, no. 1, p. 1-23, doi: 10.1016/0040-1951(95)00011-B.

Hacker, B. R., and Abers, G. A., 2004, Subduction Factory 3: An Excel worksheet and macro for calculating the densities, seismic wave speeds, and H2O contents of minerals and rocks at pressure and temperature: Geochemistry, Geophysics, Geosystems, v. 5, no. 1, doi: 10.1029/2003GC000614.

Heard, H. C. & Raleigh, C. B. 1972, Steady-State Flow in Marble at 500 to 800C. GSA Bulletin, v. 83, p. 935-956.

Hirose, K., and Kushiro, I., 1993, Partial melting of dry peridotites at high pressures: Determination of compositions of melts segregated from peridotite using aggregates of diamond: Earth and Planetary Science Letters, v. 114, no. 4, p. 477-489, doi:10.1016/0012-821X(93)90077-M.

Juračić , M., Palinkaš, L., Bajraktarević, Z., Buljan, R., Bergant, S., Jurak, V., Gušić, I., Marjanac, L., Marjanac, T., Matičec, D., Mezga, A., Paviša, T., Šestanović, S., Šoštarić-Borojević, S., Strmić, S., Sremac, J., Tišljar, J., and Vlahović, I., 2004, Adriatic-Dinaridic Mesozoic Carbonate Platform, Environments and Facies from Permian to Recent Time, *in* International Geological Congress, 32nd, Field Trip Guide Book P53, Florence – Italy, 48 p.

Karato, S.-i., and Wu, P., 1993, Rheology of the Upper Mantle: A Synthesis: Science, v. 260, no. 5109, p. 771-778, doi: 10.1126/science.260.5109.771.

Kiessling, W., Simpson, C., and Foote, M., 2010, Reefs as Cradles of Evolution and Sources of Biodiversity in the Phanerozoic: Science, v. 327, no. 5962, p. 196-198, doi: 10.1126/science.1182241.

Lapointe, P. A., 2001, Architecture of Miocene carbonate reservoirs in South East Asia: Géologie Méditerranéenne, v. 28, p. 107-109, doi: 10.3406/geolm.2001.1700.

Mackwell, S. J., Zimmerman, M. E., and Kohlstedt, D. L., 1998, High-temperature deformation of dry diabase with application to tectonics on Venus: Journal of Geophysical Research: Solid Earth, v. 103, no. B1, p. 975-984, doi: 10.1029/97JB02671.

Markello, J. R., Koepnick, R. B., Waite, L. E., and Collins, J. F., 2008, The Carbonate Analogs Through Time (Catt) Hypothesis and the Global Atlas of Carbonate Fields—A Systematic and Predictive Look at Phanerozoic Carbonate Systems, *in* Lukasik, J., and Simo, J. A., eds., Controls on Carbonate Platform and Reef Development, Volume 89, SEPM Society for Sedimentary Geology, doi: 10.2110/pec.08.89.0015.

Pall, J., Zahirovic, S., Doss, S., Hassan, R., Matthews, K. J., Cannon, J., Gurnis, M., Moresi, L., Lenardic, A., and Müller, R. D., 2018, The influence of carbonate platform interactions with subduction zone volcanism on palaeo-atmospheric CO₂ since the Devonian: Climate of the Past, v. 14, no. 6, p. 857-870, doi: 10.5194/cp-14-857-2018.

Patrulius, D., 1976, Upper Jurassic-Lower Cretaceous carbonate rocks in the eastern part of the Getic Carbonate Platform and the adjacent flysch troughs, *in* Patrulius, D., Drăgănescu, A., Baltreș, A., Popescu, B. and Rădan, S., eds, Carbonates Rocks and Evaporites: International Colloquium on Carbonates Rocks and Evaporites, Guidebook Series 15 Institute of Geology and Geophysics, Bucharest.

Pomar, L., Kendall, C. G. S. C., Lukasik, J., and Simo, J. A., 2008, Architecture of Carbonate Platforms: A Response to Hydrodynamics and Evolving Ecology, *in* Lukasik, J., and Simo, J. A., eds., Controls on Carbonate Platform and Reef Development, Volume 89, SEPM Society for Sedimentary Geology, p. 187–21, doi: 10.2110/pec.08.89.0187.

Roban, R. D., Ducea, M. N., Mațenco, L., Panaiotu, G. C., Profeta, L., Krézsek, C., Melinte-Dobrinescu, M. C., Anastasiu, N., Dimofte, D., Apotrosoaei, V., and Francovschi, I., 2020, Lower Cretaceous Provenance and Sedimentary Deposition in the Eastern Carpathians: Inferences for the Evolution of the Subducted Oceanic Domain and its European Passive Continental Margin: Tectonics, v. 39, no. 7, p. e2019TC005780, doi: 10.1029/2019TC005780.

Schlager, W., 1991, Depositional bias and environmental change—important factors in sequence stratigraphy: Sedimentary Geology, v. 70, no. 2, p. 109-130, doi: 10.1016/0037-0738(91)90138-4.

Schmid, S. M., Fügenschuh, B., Kounov, A., Maţenco, L., Nievergelt, P., Oberhänsli, R., Pleuger, J., Schefer, S., Schuster, R., Tomljenović, B., Ustaszewski, K., and Van Hinsbergen, D. J. J., 2020, Tectonic units of the Alpine collision zone between Eastern Alps and western Turkey: Gondwana Research, v. 78, p. 308-374, doi: 10.1016/j.gr.2019.07.005.

Schmid, S. M., Paterson, M. S. & Boland, J. N. 1980, High temperature flow and dynamic recrystallization in carrara marble. Tectonophysics, v. 65, p. 245-280.

Trumpy, R., 2001, Why plate tectonics was not invented in the Alps: International Journal of Earth Sciences, v. 90, no. 3, p. 477-483, doi: 10.1007/s005310000175.

Tucker, M. E., and Wright, P. V., 1990, Carbonate Sedimentology, Oxford, Blackwell Science, 482 p., doi: 10.1002/9781444314175.

Van Buchem, F. S. P., Gerdes, K. D., and Esteban, M., 2010, Mesozoic and Cenozoic carbonate systems of the Mediterranean and the Middle East: stratigraphic and diagenetic reference models - an introduction, *in* Van Buchem, F. S. P., Gerdes, K. D., and Esteban, M., eds., Mesozoic and Cenozoic Carbonate Systems of the Mediterranean and the Middle East: Stratigraphic and Diagenetic Reference Models, Volume 329: Bath, Geological Soc Publishing House, p. 1-7, doi: 10.1144/sp329.1.